JOURNAL OF CATALYSIS 134, 654–667 (1992)

Dynamic X-Ray Diffraction Study of an Unsupported Iron Catalyst in Fischer–Tropsch Synthesis

HEON JUNG AND WILLIAM J. THOMSON

Department of Chemical Engineering, Washington State University, Pullman, Washington 99164-2710

Received February 26, 1991; revised November 4, 1991

In situ, Dynamic X-Ray Diffraction (DXRD) has been used to correlate changes in bulk catalyst composition with Fischer–Tropsch activity over unsupported iron catalysts. It was found that the specific iron carbide phase formed was a function of particle size and temperature, with ε'-$Fe_{2.2}C$ formed over χ-$Fe_{2.5}C$ for smaller particle sizes and lower temperatures. While catalytic activity initially increased with the increase in carbide formation, deactivation was observed to be coincident with the $\varepsilon' \rightarrow \chi$ iron carbide transformation. This and subsequent hydrogen etching experiments indicate that the carbon formed from this transformation may act as nucleation sites for subsequent carbon deposition via the Boudouard reaction. All of the data obtained in this study are consistent with the competition model of Fischer–Tropsch synthesis, but while the carbide model does not appear to be a viable mechanism, the carbide itself may act as the catalyst.

INTRODUCTION

It is well known that the bulk phase of iron catalysts is converted to carbides under typical Fischer–Tropsch (FT) reaction conditions. Arguably at least five different iron carbides are known to exist during the FT synthesis: "O-carbides" (carbides with carbon atoms in octahedral interstices; ε-Fe_2C, ε'-$Fe_{2.2}C$, and Fe_xC) and "TP-carbides" (carbides with carbon atoms in trigonal prismatic interstices; χ-$Fe_{2.5}C$ and Fe_3C) (*1, 2*). The formation and distribution of these phases are sensitive functions of reaction conditions, reaction time and the physiochemical state of the catalyst (supported or unsupported, reduced or unreduced, etc.). However, the specific role played by these carbide phases during the synthesis has not been clearly resolved. For example, the observation that iron carbide phases form simultaneously with the initial slow increase in catalyst activity has brought about two different models to account for this time-dependent behavior. In the "carbide model," iron is not active and the actual catalytic activity occurs on active surface sites located on the bulk carbide phase where the degree of bulk carburization controls the active site density (*3, 4*). *In situ* Mössbauer spectroscopy work by Raupp and Delgass showing the almost linear relationship between the FT activity (*3*) and the extent of the bulk carbide formation is good evidence for the validity of the carbide model. On the other hand, in the "competition model," iron atoms on the surface are taken to be the active sites and there is a competition between the diffusion of carbon into the bulk (to form carbide) and the hydrogenation of carbon to form hydrocarbons (*2, 5*). Several experimental observations (*6–8*) are consistent with the competition model, including Niemantsverdriet *et al.*'s observation that the maximum FT activity was reached well before all iron had been carbided (*2*).

Because of the sensitivity of the carbide formation to the specific reaction conditions (reaction temperature, gas composition, and the particle size of initial iron), the different observations made by Raupp and Delgass (*3*) and Niemantsverdriet *et al.* (*2*) may be attributed to the different experimental con-

0021-9517/92 $3.00

ditions employed by these authors. This points to the necessity of simultaneously investigating the effect of reaction conditions on both the carburization and FT activity.

It has also been reported that the composition of the iron carbide phases changes during long FT synthesis periods, depending on the stability of each carbide phase at the reaction temperature (*2, 9, 10*). During this period, catalysts typically experience a decrease in FT activity. Although it is probable that there is a relation between the transformation of the carbide phases and deactivation, no attempt has been made to relate these two phenomena. The recent proposal of De Bokx and co-workers (*11–13*) that carbon filaments grow by the decomposition of the metastable carbide in both Ni and Fe catalysts adds to the interest in investigating the mechanism of the deactivation of FT synthesis over iron catalysts. A simultaneous, *in situ,* reaction and solid phase characterization technique is ideally suited to investigate questions of this nature.

Characterization techniques such as Mössbauer spectroscopy (MES), X-ray diffraction (XRD), and thermomagnetic analysis have been used to study changes in the bulk phase of iron catalysts. Even though many results have been published using MES, some of the quantitative MES data are not reliable since the proportions of the carbide phases which are determined by MES are a function of the observation temperature (*14*). In fact, the most reliable data are obtained at 4 K (*15*).

Even with the criticism that XRD cannot determine the structures of so-called O-carbides (*1*), XRD can differentiate O-carbides from TP-carbides (*2*), although it must be kept in mind that XRD measurements are only representative of bulk compositions. In fact, *in situ* XRD with a dynamic capability, dynamic X-ray diffraction (DXRD) (*16, 17*), has demonstrated its effectiveness in both the quantitative and qualitative characterization of the kinetic behavior of the reduction/oxidation of supported and unsupported iron catalysts (*18*).

In this study *in situ* DXRD was used to investigate the kinetic behavior of the carburization of unsupported iron during FT synthesis. In particular, the effect of several variables (iron particle size, reaction temperature, and gas composition) on the FT activity and the rate of carburization was examined. Data are also obtained on the transformation of the carbide phases during both FT synthesis and hydrogen etching, and the results are interpreted in terms of the mechanism of the deactivation.

EXPERIMENTAL

Materials

The catalyst was prepared by drying $Fe(NO_3)_3 \cdot 9H_2O$ (Mallincrodt) in air at 383 K for 48 h followed by calcining in air at 623 K for 24 h. BET area and the pore volume were measured by N_2 adsorption (Autosorb 6, Quantachrome) and are 20.3 m^2/g and 0.110 cm^3/g, respectively. Gases used in this study were high purity grade and were used after passing through a deoxo unit and then a molecular sieve trap.

DXRD

The specific details of the DXRD equipment have been given elsewhere (*16–18*), but it consists of a Siemens D500 θ–2θ powder diffractometer equipped with a flow-through, Anton–Paar hot stage and a position-sensitive detector capable of rapid scanning (60 deg/min) at high resolution (0.01 degrees). Co$K\alpha$ radiation and an iron filter were used in all of the experiments reported here. A thin (less than 0.3 mm) sample of powdered catalyst (diameter of about 10 μm) of about 100 mg was placed on a platinum strip which was electrically heated. A type S thermocouple, attached to the strip, serves as a temperature monitor and is used to control the temperature or heating program by means of Micristar Model 828D controller. Tracer tests of the hot stage reaction chamber indicate that it behaves similarly to a perfect back-mixed reactor. Gases from the reaction chamber were analyzed by GC (Carl 111H equipped

with a hydrogen transfer system and with molecular sieve 13X and Porapak Q columns) as well as continuously by two nondispersive infrared (NDIR) analyzers (CO_2 and CH_4, Beckman and Horiba, respectively).

Procedures

Two different reduction conditions were employed to control the particle size of the reduced iron; high-temperature reduction (573 K, 2 h in H_2) and low-temperature reduction (543 K, 4 h in H_2). At the end of the reduction, XRD scans were used to estimate the particle size of iron by X-ray line broadening analysis (XLBA). Average particle sizes were calculated using Scherrer's formula with Warren's correction (*19*). After the XRD scan, the sample temperature was adjusted to the desired reaction temperature in flowing hydrogen, followed by a change to the FT synthesis gas mixture, once the desired temperature was reached (typically, in 20 s). The gas mixture was supplied at a high flow rate (500 ml–min) for 1 min to enhance the initial mixing inside the chamber and then adjusted to about 100 ml/min. Reaction runs were carried out at atmospheric pressure and at three different temperatures (503, 523, and 543 K). In most of the runs, a 3.2 H_2–CO gas mixture was used. Selective experiments were also conducted with H_2–CO mixtures of 0.84 and 7.0. DXRD scans were performed at appropriate time intervals during the run, and quantitative analysis of the DXRD data was accomplished by using the "External Standard Method" (*20*) to determine the weight fractions of each phase (iron and carbide). After a particular reaction period (0.33 to 20 h), pure hydrogen gas was supplied at a flow rate of about 200 ml/min, and the temperature was raised to 623 K in 30 s. During this phase of the experiment, hydrogen etching of the catalyst took place and was monitored using both DXRD and gas analyses. A differential packed bed reactor was also used with the same procedure to compare the activity behavior of the DXRD runs.

Reduced samples were also subjected to CO chemisorption measurements using a pulse technique at 77.7 K. The total adsorption (chemisorption and physical adsorption) of CO was corrected for the quantity due to physical adsorption by measuring the amount of desorbed CO when the sample temperature was raised to 195 K. The difference between the two gives the chemisorbed amount of CO. Reduced iron surface areas determined by CO chemisorption (area occupied by a CO molecule on an Fe surface = 12 Å) were 29.8 and 54.9 m^2/g for the iron reduced at 573 K and for that reduced at 543 K, respectively.

RESULTS AND DISCUSSIONS

The catalyst was scanned by XRD after the calcination step and was found to be in the form of α-Fe_2O_3 (hematite) with an average particle size estimated to be 22 nm from XLBA. The reduction condition influences the size of the reduced iron particles due to sintering during the reduction (*21*). The reduction of the unsupported hematite at two different temperatures resulted in different particle sizes. The averages sizes of iron from the high-temperature reduction (573 K) and the low-temperature reduction (543 K) were estimated by XLBA to be 30 nm and 16 nm, respectively. The decrease in particle size from 22 nm to 16 nm as hematite was reduced to iron at 543 K is not surprising since the oxygen atoms removed from the oxide lattice create microporosity during the reduction process (*21*). Iron particle sizes calculated from the CO chemisorption measurement (assuming spherical particles) also yielded comparable values of 26 nm and 14 nm after high- and low-temperature reduction, respectively.

Carbide Formation

Figure 1 shows a typical DXRD spectra demonstrating the conversion of iron to carbides during the Fischer–Tropsch reaction; in this case for the catalyst reduced at the lower temperature. Zero time corresponds to the point when the 3.2H_2/CO gas mixture was introduced into the hot stage chamber.

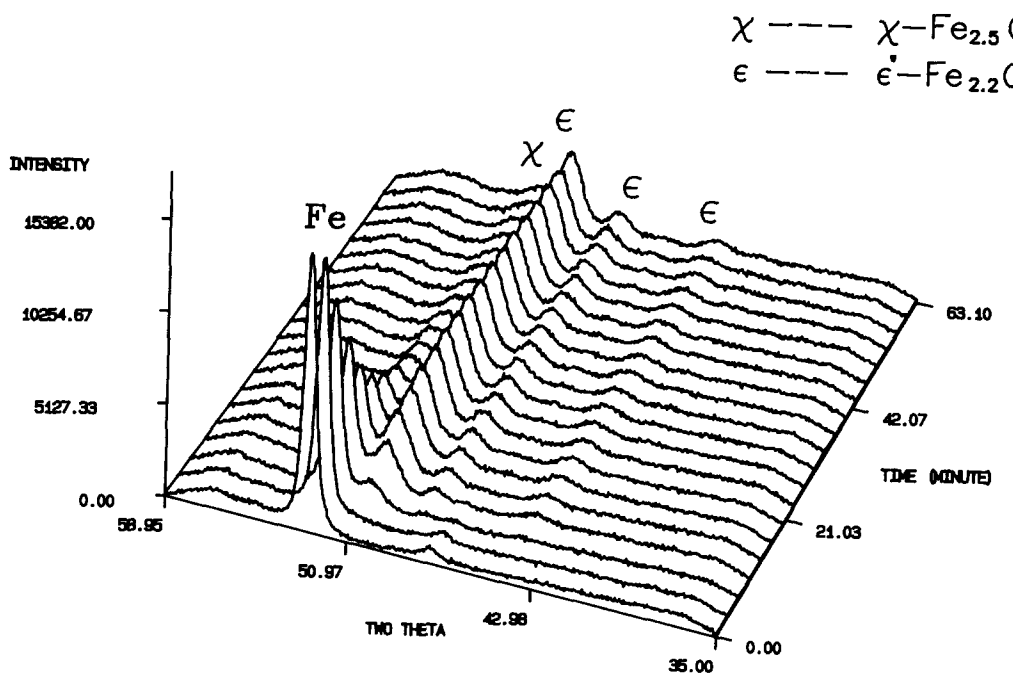

FIG. 1. DXRD carburization data for iron reduced at 543 K (16-nm iron particles, T = 523 K, H_2/CO = 3.2).

The carbide phases formed in this case were mostly ε'-$Fe_{2.2}C$ with only minor quantities of χ-$Fe_{2.5}C$ and its XRD spectra is shown in Fig. 2b below. Four types of carbides have been reported to form during FT synthesis over unsupported iron at the temperatures used in this study: ε-Fe_2C, ε'-$Fe_{2.2}C$, Fe_xC, and χ-$Fe_{2.5}C$ (*1, 2*). However, the interpretation of the MES spectra of ε'-$Fe_{2.2}C$ and ε-Fe_2C needs very careful evaluation in order to obtain quantitative significance (*22*). In addition, the existence of ε-Fe_2C and Fe_xC are also in question (*1*). While the XRD pattern of χ-$Fe_{2.5}C$ has been well established (*23, 24*), there seems to be very little difference in the diffraction patterns between ε-Fe_2C and ε'-$Fe_{2.2}C$. This is not too surprising since they have the same structure and very small differences in their stoichiometry. In fact, the XRD pattern of ε-Fe_2C reported by Barton and Gale (*25*) was later corrected to be that of ε'-$Fe_{2.2}C$ by Niemantsverdriet *et al.* (*2*). Because it is not possible to distinguish between ε-Fe_2C and ε'-$Fe_{2.2}C$ by XRD, we chose to follow the assignment made by Niemantsverdriet *et al.* (*2*) and thus we have designated this carbide phase as ε'-$Fe_{2.2}C$. Figure 2 shows DXRD spectra which were measured during exposure of the two catalysts to different temperatures. The XRD spectra corresponding to the ε' and χ carbide phases are shown in Fig. 2a. These spectra were obtained when the catalyst with the smaller iron particles was exposed to synthesis gas at 503 K (solid spectra) and subsequently heated to 623 K in synthesis gas (dashed spectra). They are in excellent agreement with the reported spectra for ε'-$Fe_{2.2}C$ (*2, 25*) and χ-$Fe_{2.5}C$ (*23, 24*), respectively.

Because, in this case the major peaks of iron (2θ = 52.29), ε'-carbide (2θ = 50.34), and χ-carbide (2θ = 50.89, 51.72) are so close to one another it was impossible to quantify the composition by integrating the intensities. Instead, maximum peak intensi-

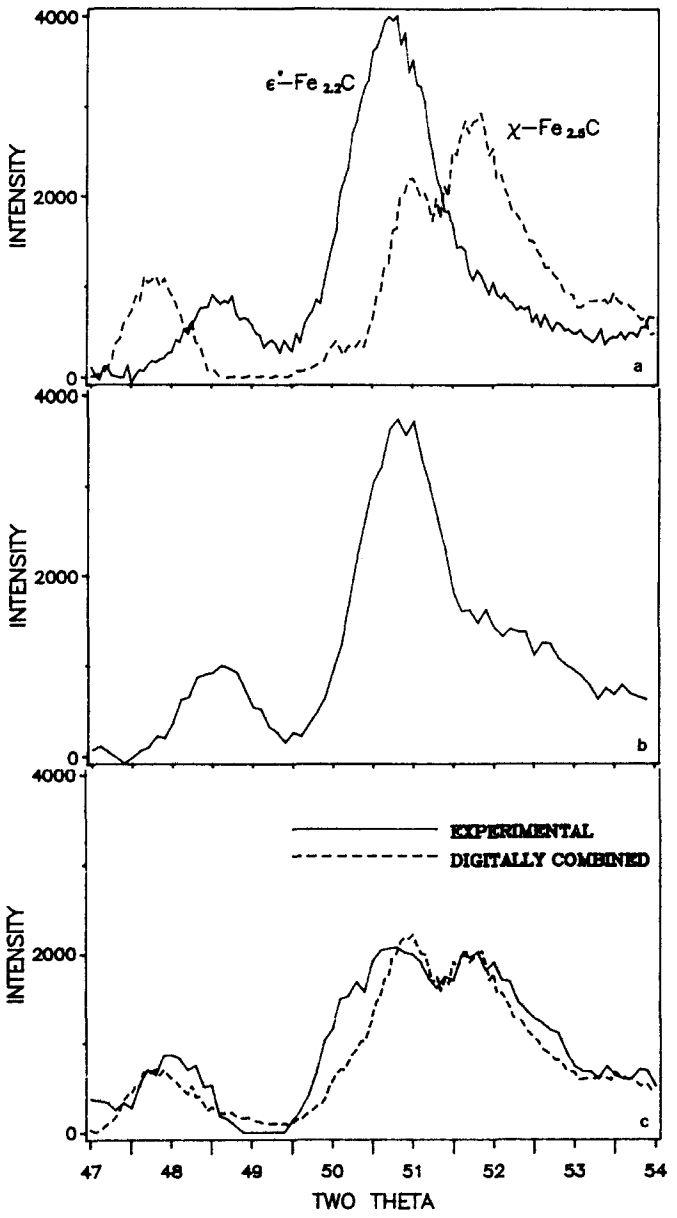

FIG. 2. XRD peaks of carbides formed from reduced iron ($H_2/CO = 3.2$); (a) ε'-$Fe_{2.2}C$ (carbide formed at 503 K from 16-nm iron particles) and χ-$Fe_{2.5}C$ (carbide formed by heating ε'-$Fe_{2.2}C$ to 623 K); (b) carbide formed at 523 K from 16-nm iron particles; (c) carbide formed at 523 K from 30-nm iron particles (solid spectra) and digitally combined spectra of 30% ε'-$Fe_{2.2}C$ and 70% χ-$Fe_{2.5}C$ (dashed spectra).

ties of iron with correction for the overlapping carbide intensities were used. The use of the maximum intensity instead of the integrated intensity is justified by the linear relation between them, as shown in Fig. 3, which shows the maximum intensity of iron plotted versus the corresponding integrated intensity during the reduction of Fe_3O_4 to Fe. Because of this correlation, the values calculated for carbide fractions (which are

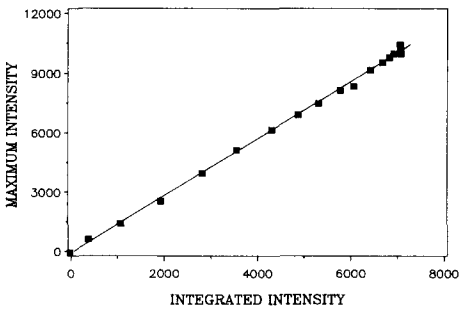

FIG. 3. Comparison of maximum peak intensity of iron and integrated intensity of iron during the reduction of iron oxide (T = 573 K in H_2).

based on the Fe peak measurements) are considered to be quantitative. However the data related to the specific carbide phases (for example, in Fig. 7) are only semiquantitative but are only intended to illustrate *changes* in composition.

Using this method, the degree of total carburization of iron at three different temperatures and two particle sizes are shown in Fig. 4. As expected, the smaller iron particles (16 nm) converted to carbides faster than the larger ones (30 nm). Similar observations were made by Raupp and Delgass (*9*) on supported iron catalysts. It can also be seen in Fig. 4 that, at higher reaction temperatures, higher carburization rates are observed, and there is a diminished effect of particle size.

During the course of this study, it was also found that the type and composition of the carbide phases which formed after complete carbide formation were a function of both iron particle size and reaction temperature (Fig. 2). The effect of temperature is clearly evident in Fig. 2a, where the ε'-carbide formed at 503 K is seen to transform to the χ-carbide when the temperature is raised to 623 K. In addition, the XRD spectra in Fig. 2b shows the appearance of small quantities of χ-carbide mixed with ε'-carbide when the catalyst is exposed to synthesis gas at a slightly higher temperature of 523 K. The effect of particle size can be seen in comparing Figs. 2b and c. At this point in the experimental run, the DXRD data clearly showed the disappearance of elemental iron in both cases and the spectra in Fig. 2c correspond to a mixture of approximately 30% ε'-carbide and 70% χ-carbide. The latter was arrived at by digitally combining 30% and 70% of the XRD spectra shown in Fig. 2a for the ε'-carbide and χ-carbide, respectively. As can be seen, this combination (dashed spectra) provides a good match to the observed experimental data (solid spectra). It is evident, therefore, that χ-$Fe_{2.5}C$ is more stable when ε'-$Fe_{2.2}C$ and that χ-$Fe_{2.5}C$ is preferentially formed on larger particles. Similar conclusions relative to the effect of particle size were reached by Raupp and Delgass for supported iron catalysts. Using MES, they found that small iron particles (6.1–7.4 nm) supported on silica favored the formation ε'-$Fe_{2.2}C$, while larger particles (10.1 nm) formed χ-$Fe_{2.5}C$ at 523 K (*9*). Although there has been no previous reported work on the effect of particle size on carbide formation on unsupported iron catalysts, Niemandtsverdriet *et al.* found that unsupported iron (30-nm particles) formed a mixture of ε'-$Fe_{2.2}C$ and χ-$Fe_{2.5}C$ at 513 K. They also suggested that the nature of the catalyst (promoted or supported) is critical to the process which determines the type of carbide formed (*2*). However, it was found in this study that, as with supported iron catalysts, iron particle size alone can also determine the specific carbide phase which is formed on unsupported iron. That is, the smaller iron particles (16 nm) formed pure ε'-$Fe_{2.2}C$, while the same unsupported iron with a larger particle size (30 nm) formed a mixture of ε' and χ-carbide at 503 K. It should be pointed out that after complete carburization, ε'-$Fe_{2.2}C$ continuously transformed to χ-$Fe_{2.5}C$, also indicating the instability of ε'-carbide.

Figure 5 shows the effect of the synthesis gas mixture ratio on the total carburization rate of the 30-nm iron particles. As can be seen, iron particles carburized at a much slower rate when the ratio of H_2/CO was higher. However, when the ratio of H_2/CO

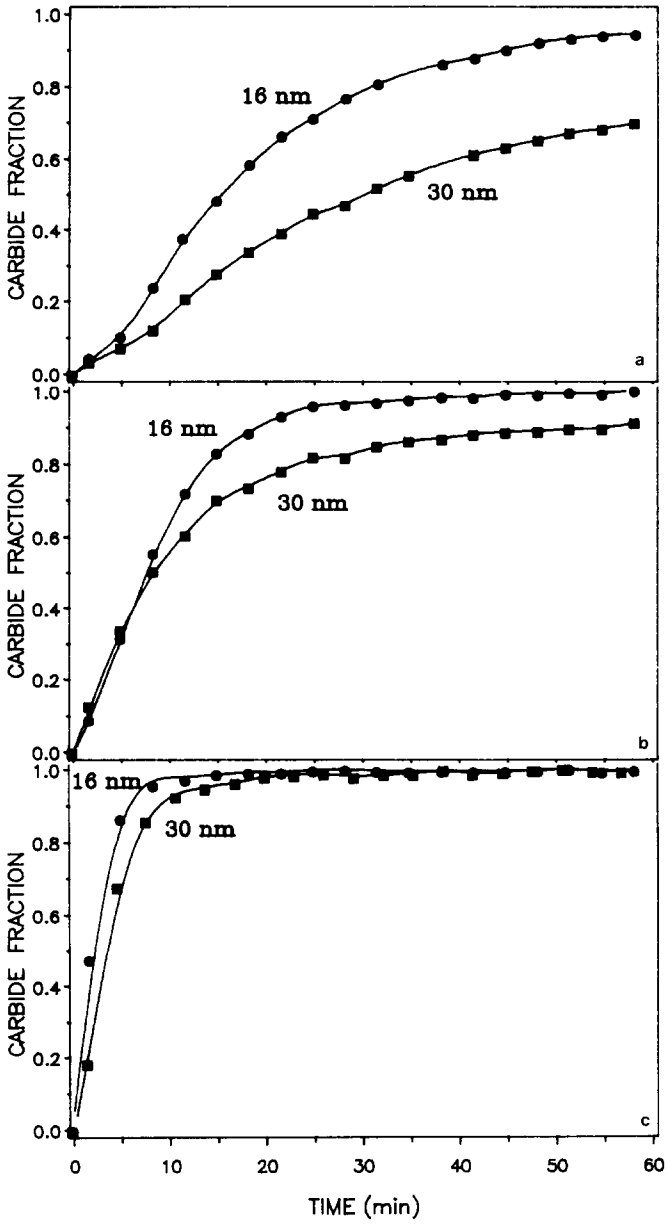

FIG. 4. Carburization rates of iron; (a) at 503 K, (b) at 523 K, and (c) at 543 K (H_2/CO = 3.2).

was less than 3.2, its effect on the carbide formation rate was slight.

FT Synthesis Activity

Several runs of FT synthesis were carried out in a differential packed bed reactor to demonstrate that the bulk characterization of the catalysts during *in situ* DXRD is representative of the actual behavior. There was very good agreement in terms of the magnitude and time dependency of the reaction rate measured in the DXRD chamber with that measured in the packed bed reactor. Since the conversions were typically

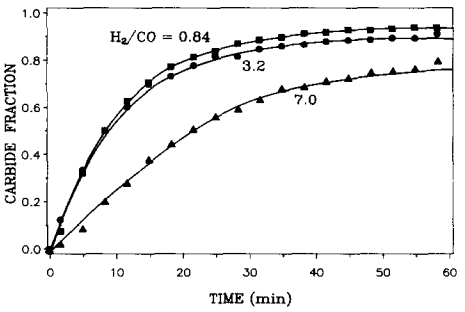

FIG. 5. Effect of gas composition on carburization rates (30-nm iron, T = 523 K).

about 1% or less, the DXRD reaction chamber can be regarded as a differential reactor in which heat and mass transfer effects are very small. Because of the low conversion, only hydrocarbons up to C_3 were produced in a measurable quantity by GC. Typical product distributions were: C_2/C_1 = 0.72, C_3/C_1 = 0.09, $C_2^=/C_2$ = 1.2, and $C_3^=/C_3$ = 0.43. However, in order to relate the catalyst activity to changes in the bulk catalyst, only the methane formation rate was used as a measure of the catalyst activity.

Typical changes in the FT activity over the reduced iron, as measured in the DXRD chamber, are shown in Fig. 6 for both iron particle sizes. Consistent with previous observations, the iron catalysts exhibited a gradual increase in activity to a maximum followed by a gradual loss in activity. As can be seen, both the activation and the deactivation are strong functions of the reaction temperature, but only slightly dependent on particle size. The data in Figs. 4 and 6 are combined in Fig. 7, in this case for the small iron particles (16 nm), in order to demonstrate that the bulk iron phase was converted to carbides during the activation period at all of the temperatures tested. It should be pointed out that the XRD peak intensities in Fig. 7 are for ε'-$Fe_{2.2}C$, since most of the carbide phase formed from the smaller iron particles was ε'-$Fe_{2.2}C$ and was found to be directly proportional to the degree of total carbide formation. At the time when the intensity of ε'-$Fe_{2.2}C$ reached a maximum, iron particles were shown to be completely carburized from the time resolved DXRD spectra. As can be seen in Fig. 7, the activity increase and the change in the degree of bulk carburization are almost linearly related up to the point of complete carburization for the small particles at all three temperatures. These results for the small particles are consistent with both the carbide (*3*) and the competition model (*5*). However, for the larger iron particles (30 nm in size), the catalyst began to deactivate before complete carburization at all three temperatures. For example, catalytic activity reached a maximum at about 90% of complete carburization for the large iron particles at 523 K, whereas there was a direct correlation of activity with carburization for the 16 nm iron particle (compare Fig. 7b and Fig. 8b below). These results suggest that the discrepancy between catalyst activity and degree of carbide formation observed by Raupp and Delgass (*3*) and by Niemantsverdriet *et al.* (*2*) is due to the differences in the size of their iron particles. Raupp and Delgass, using iron supported on silica or magnesia, reported particle sizes between 6 and 17 nm, while the unsupported iron tested by Niemantsverdriet *et al.* had particle sizes of about 30 nm. It should be pointed out that these results alone cannot refute the carbide model, since the bulk XRD measurements may not reflect the composition at the surface. For example, if the particles are sufficiently large, the rate of carburization in the particle interior will become carbon-diffusion limited and the diffusion rate may not be sufficient to support formation of the ε'-carbide phase in the bulk. Nevertheless, these results are consistent with the competition model and, as discussed below, the competition model is also supported by the effect of CO pressure.

The results in Fig. 8, which show changes in activity and the degree of carburization in different gas atmospheres, can be explained very well by the competition model. Recall that, in the competition model, the formation of surface carbidic carbons is postu-

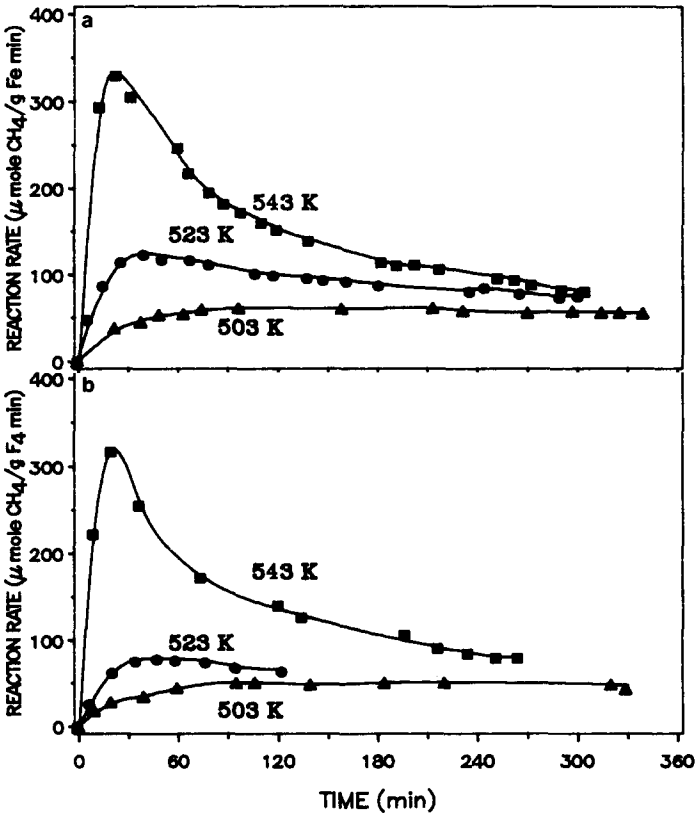

FIG. 6. Rate of CH_4 formation during FT synthesis as a function of time; (a) 16-nm iron particles, (b) 30-nm iron particles (H_2/CO = 3.2).

lated to be the common precursor for both diffusion of carbon into the bulk iron and for hydrocarbon formation. As can be seen in Fig. 8, carbides form at a slower rate as the H_2/CO ratio increases, which is expected because of the lower partial pressure of CO. Moreover, because of the higher partial pressures of H_2, more hydrogen competes for the carbidic carbon, resulting in a lower carburization rate. As the ratio of H_2/CO decreases, more surface carbon forms initially on the surface (less competition) which is then available for diffusion into the bulk, leading to higher carburization rates (Fig. 8b). In the case of very low H_2/CO, too much surface carbon forms in the early stage of reaction leading to early deactivation by forming inactive surface carbons (Fig. 8c). The latter conclusion is based on the observation that the rate of deactivation was highest at the lowest H_2/CO ratio, but the carburization rate was almost the same (Fig. 5). This also suggests that the rate determining step for carburization may be the reaction of carbon with the bulk iron.

Even though the observations in this study, together with those of previous studies (*2*, *6–8*) are consistent with the competition model, the model has one controversial point; i.e., whether iron atoms or surface carbides are the active sites. Although surface iron atoms are not likely to exist once the iron is completely carbided, iron carbide still exhibited FT activity. Even though the carbide forms from the surface during the carburization (*26*), it is still possible that the surface carbide regenerates iron by reacting with hydrogen gas to form CH_4. However,

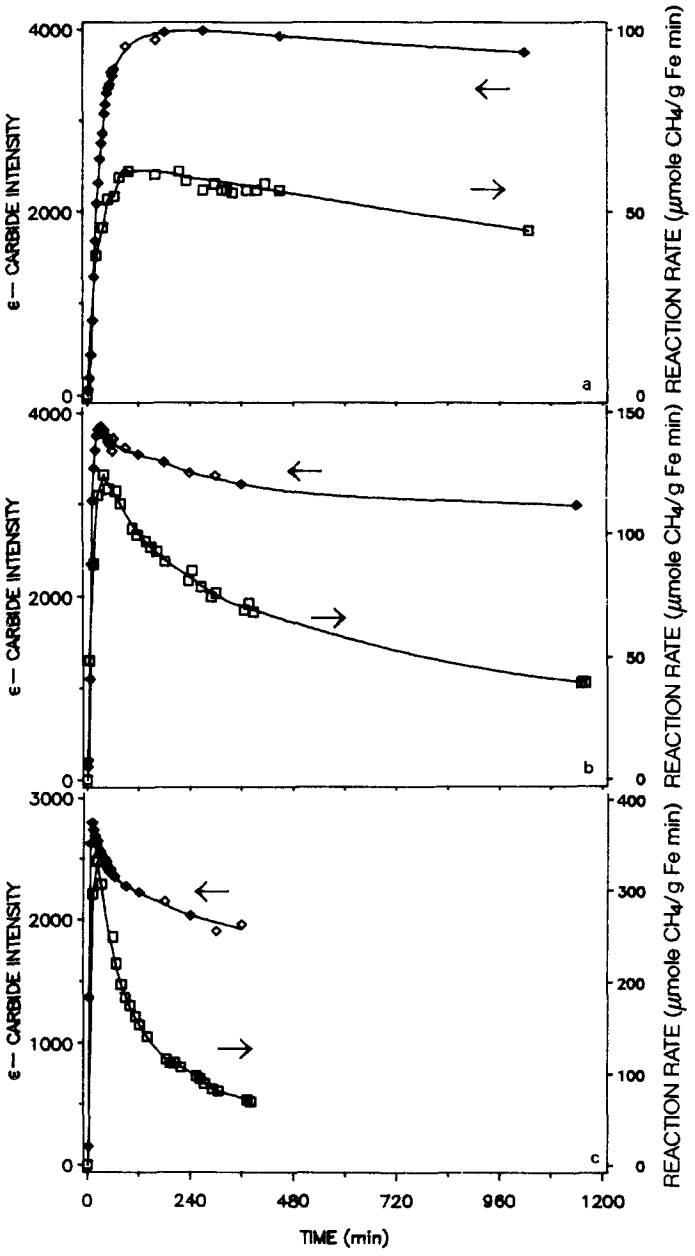

FIG. 7. Effect of temperature on degree of carburization and activity change during FT reaction; (a) at 503 K, (b) at 523 K, (c) at 543 K, (H_2/CO = 3.2, 16-nm iron particles).

an *in situ* IR study of CO adsorption on a spent Fe/Al_2O_3 catalyst failed to show CO adsorption bands, which are characteristic of CO associated with iron in the metallic state (*27*). In another study, preoxidized iron foils were observed to have a high FT activity (*28*) and this was taken to be supporting evidence for the validity of the competition model; i.e., by assuming the freshly reduced iron on the oxide surface is active

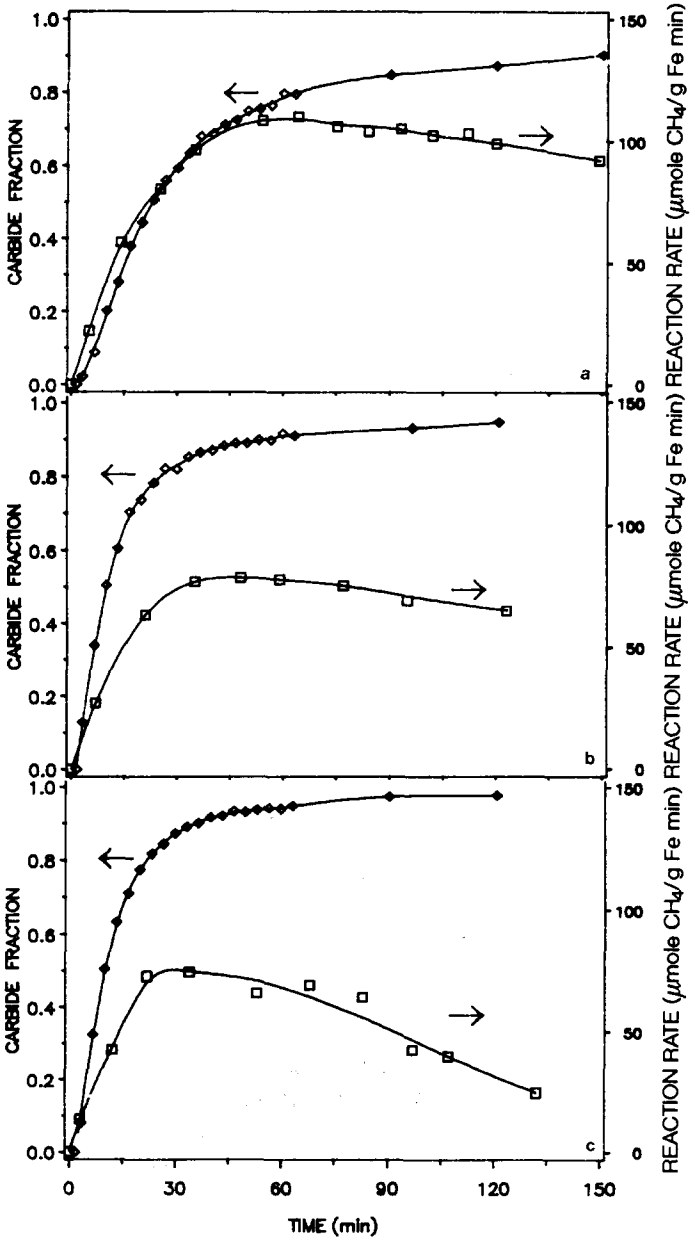

FIG. 8. Effect of synthesis gas composition on degree of carburization and activity change during FT reaction; (a) $H_2/CO = 7.0$, (b) $H_2/CO = 3.2$, (c) $H_2/CO = 0.84$ ($T = 523$ K, 30-nm iron particles).

(*5*, *28*). However, it is also possible that freshly reduced iron can form carbides rapidly. In fact, unreduced α-Fe_2O_3 has been tested as a catalyst in FT synthesis and had high activities with bulk compositions of Fe_3O_4 and χ-$Fe_{2.5}C$ and in the absence of iron (*29–31*). Previous workers are divided in their opinion as to whether Fe_3O_4 (*29*, *30*), and/or iron or carbide is active (*31*). It follows from the above argument that the iron carbide phase cannot be ruled out as an active species for FT synthesis.

The importance of the specific carbidic phase present on the catalyst may also be important. For the small Fe particles, the intensity of ε'-$Fe_{2.2}C$ decreased after complete carburization and was accompanied by a decrease in the FT activity (Fig. 7). The DXRD data also showed that the decrease of the ε'-$Fe_{2.2}C$ phase occurred simultaneously with an increase of the χ-$Fe_{2.5}C$ phase, indicating that an ε'-carbide–χ-carbide transformation takes place. It should be also pointed out that even the larger iron particles, which initially form a mixture of ε'-$Fe_{2.2}C$ and χ-$Fe_{2.5}C$, also underwent an ε'-carbide–χ-carbide transformation during the deactivation period even though carburization was incomplete. The stability of iron carbides is known to increase as carbon concentration decreases (*1*); that is

$$\varepsilon'\text{-}Fe_{2.2}C < \chi\text{-}Fe_{2.5}C < \theta\text{-}Fe_3C.$$

The rate of the ε'-carbide–χ-carbide transformation is higher at higher reaction temperatures, due to the instability of ε'-carbide at higher temperatures, and this is coincident with increases in the deactivation rate (Fig. 7).

It is possible that the ε'-carbide–χ-carbide transformation is strongly related to the deactivation of iron FT synthesis catalysts. While the formation of inactive carbon on the surface of catalysts is generally accepted as the cause of deactivation in FT synthesis (*2, 28, 29*), the mechanism of inactive surface carbon formation has not been studied thoroughly. It should be noted that the decomposition of metastable ε'-$Fe_{2.2}C$ can also lead to a buildup of inactive carbon,

$$2.5Fe_{2.2}C \rightarrow 2.2Fe_{2.5}C + 0.3C,$$

which then blocks the active sites of the catalyst. The carbon which results from the decomposition seems to serve as the nucleation site for the further buildup of the inactive surface carbon. This hypothesis is supported by the work of De Bokx and coworkers (*11–13*). They reported that carbon filaments grow by the continuous decomposition of metastable carbide intermediates in both Ni and Fe catalysts. Their results agree very well with the observation in this study that the ε'-carbide–χ-carbide transformation could be a primary cause of FT deactivation.

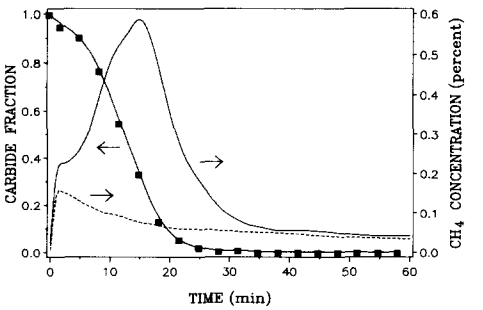

FIG. 9. CH_4 evolution and decarburization during H_2 etching at 623 K; total CH_4 evolution (solid line), CH_4 from hydrogenation of non-carbidic surface carbon (dotted line) (16-nm iron particles, exposed to FT synthesis for 19.5 h at 523 K in 3.2 H_2/CO).

Hydrogen Etching

Immediately following a DXRD FT synthesis experiment, the gas stream was changed to pure hydrogen in order to "etch" carbon from the catalyst. Since the catalysts decarburized (carbide → iron) very slowly at the original reaction temperatures (503–543 K), all of the etching experiments were carried out at 623 K. During the etching experiments, carbide decarburization and methane evolution were measured by DXRD and CH_4-NDIR, respectively.

Figure 9 shows the isothermal change of carbide to iron along with the simultaneous change in the concentration of evolved CH_4 during hydrogen etching of the 16-nm catalyst sample after it had been exposed to a gas stream of 3.2 H_2/CO for 19.5 h at 523 K. It should be pointed out that on heating the sample to 623 K, the remaining ε'-$Fe_{2.2}C$ transformed completely and very rapidly to χ-$Fe_{2.5}C$, indicating the instability of ε'-$Fe_{2.2}C$ at 623 K. As can be seen in Fig. 9, the peak of evolved CH_4 concentration corresponds very well to the hydrogenation of the carbide phase (decarburization). How-

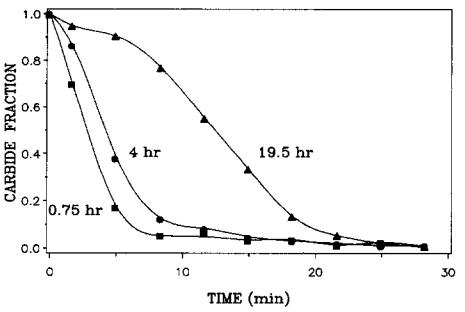

FIG. 10. Decarburization rates of the catalysts used for different periods of FT reaction (16-nm iron particles, exposed to FT synthesis at 523 K in 3.2 H_2/CO).

ever, there is a rapid increase in CH_4 evolution at the beginning of the etching experiment, when there is almost no decarburization, and a slow, steady evolution even after complete decarburization. The solid line in CH_4 evolution curve is the sum of the CH_4 evolved from the decarburization of carbide and the CH_4 produced from the hydrogenation of surface carbons, both of which are produced simultaneously. The dotted line in Fig. 9 corresponds to the methane produced by hydrogen gasification of the non-carbidic carbon. It was calculated by subtracting the methane corresponding to decarburization ($Fe_{2.5}C + 2H_2 \rightarrow 2.5Fe + CH_4$) from the total methane evolved.

Catalysts which were exposed to FT synthesis for different periods were also subjected to hydrogen etching, and the decarburization kinetic results are shown in Fig. 10. The catalysts used for a longer period of time experienced a greater degree of deactivation, and as Fig. 10 shows, that catalysts exposed to longer reaction periods decarburized slower than catalysts which experienced shorter reaction periods. In fact, in the case of a highly deactivated catalyst (543 K for 10 h in FT synthesis), decarburization was so slow that only after 4 h of hydrogen etching did it start to decarburize, while steadily producing small quantities of methane from the hydrogenation of non-carbidic surface carbon. Based on these results, it is apparent that it is the inactive surface carbon which causes FT catalyst deactivation. In all cases where deactivation is more severe (longer exposure times, higher temperatures) the rate of decarburization by hydrogen was lower. This is undoubtedly due to the non-carbidic carbon inhibiting contact between H_2 and the carbide. Based on these results and the fact that the $\varepsilon'-\chi$ transformation coincides with FT deactivation, it is possible that the carbon produced from the phase transformation acts as nucleation sites for the formation and/or polymerization of carbon from the Boudouard reaction ($2CO \rightarrow C + CO_2$).

CONCLUSIONS

Based on the *in situ*, DXRD Fischer–Tropsch experiments conducted here over unsupported iron, a number of conclusions can be drawn. The carburization rate of iron during the FT reaction was found to be a function of the reaction temperature, the iron particle size, and the H_2/CO ratio. The reduction conditions (temperature and duration) changed the reduced iron particle sizes significantly due to sintering, even at 573 K. During the carburizing phase of FT synthesis, the unsupported iron with an average particle size of 16 nm formed exclusively ε'-$Fe_{2.2}C$, while the unsupported iron with a 30-nm particle size formed a mixture of ε'-$Fe_{2.2}C$ and χ-$Fe_{2.5}C$ at temperatures lower than 523 K. The relationship between FT activity change and carbide formation is better explained by the competition model, although carbide itself cannot be totally ruled out as the catalytic species. The observation that the decomposition of metastable ε'-$Fe_{2.2}C$ to χ-$Fe_{2.5}C$ was coincident with deactivation, and post-reaction hydrogen etching experiments suggest that the deactivation of the iron catalyst during FT synthesis is caused by the buildup of non-carbidic surface carbons via the ε'-$Fe_{2.2}C$ to χ-$Fe_{2.5}C$ transformation. That is, the carbon produced by this transformation may act as nucleation sites for the subsequent deposition of non-carbidic carbon from the Boudouard reaction.

ACKNOWLEDGMENT

This material is based upon work supported by the National Science Foundation under Grant CBT-8719929. The Government has certain rights in this material.

REFERENCES

1. Le Caer, G., Dubois, J. M., Pijolat, M., Perrichon, V., and Bussiere, P., *J. Phys. Chem.* **86,** 4799 (1982).
2. Niemantsverdriet, J. W., van der Kraan, A. M., van Dijk, W. L., and van der Baan, H. S., *J. Phys. Chem.* **84,** 3363 (1980).
3. Raupp, G. B., and Delgass, W. N., *J. Catal.* **58,** 361 (1979).
4. Matsumoto, H., *J. Catal.* **86,** 201 (1984).
5. Niemantsverdriet, J. W., and van der Kraan, A. M., *J. Catal.* **72,** 385 (1981).
6. Matsumoto, H., and Bennett, C. O., *J. Catal.* **53,** 331 (1978).
7. Amelse, J. A., Schwartz, L. H., and Butt, J. B., *J. Catal.* **72,** 95 (1981).
8. Reymond, J. P., Meriaudeau, P., Pommier, B., and Bennett, C. O., *J. Catal.* **64,** 163 (1980).
9. Raupp, G. B., and Delgass, W. N., *J. Catal.* **58,** 348 (1979).
10. Tau, L. M., Borcar, S., Bianchi, D., and Bennett, C. O., *J. Catal.* **87,** 36 (1984).
11. De Bokx, P. K., Kock, A. J. H. M., Boellaard, E., Klop, W., and Geus, J. W., *J. Catal.* **96,** 454 (1985).
12. Kock, A. J. H. M., De Bokx, P. K., Boellaard, E., Klop, W., and Geus, J. W., *J. Catal.* **96,** 468 (1985).
13. Boellaard, E., De Bokx, P. K., Kock, A. J. H. M., and Geus, J. W., *J. Catal.* **96,** 481 (1985).
14. Amelse, J. A., Grynkewich, G., Butt, J. B., and Schwartz, L. H., *J. Phys. Chem.* **85,** 2484 (1981).
15. Niemantsverdriet, J. W., Flipse, C. F. J., van der Kraan, A. M., and van Loef, J. J., *Appl. Surf. Sci.* **10,** 302 (1982).
16. Anderson, D. E., and Thomson, W. J., *Ind. Eng. Chem. Res.* **26,** 1628 (1987).
17. Thomson, W. J., *Ceramic Transactions* **5,** 131 (1989).
18. Jung, H., and Thomson, W. J., *J. Catal.* **128,** 218 (1991).
19. Klug, H. P., and Alexander, L. E., "The X-Ray Diffraction Procedures: For Polycrystalline and Amorphous Materials," 2nd ed. Wiley, New York, 1974.
20. Cullity, B. D., "Elements of X-Ray Diffraction." Addison–Wesley, Reading, 1978.
21. Themelis, N. J., and Gauvin, W. H., *Trans. Am. Inst. Min. Metall. Pet. Eng.* **227,** 290 (1963).
22. Gatte, R. R., and Phillips, J., *J. Catal.* **104,** 365 (1987).
23. Jack, K. H., *Proc. R. Soc. London Ser. A* **195,** 56 (1948).
24. Hofer, L. J. E., Cohn, E. M., and Peebles, W. C., *J. Am. Chem. Soc.* **71,** 189 (1949).
25. Barton, G. H., and Gale, B., *Acta Crystallogr.* **17,** 1460 (1964).
26. Biryukovich, M. M., Rozovskii, A. Y., Ivanov, A. A., Liberov, L. G., Butyugin, V. K., Kagan, Y. B., Kryukov, Y. B., and Bashkirov, A. N., *in* "Surface Interactions between Metals and Gases" (V. I. Arkharov and K. M. Gorbunova, Eds.), p. 67. Consultants Bureau, New York, 1966.
27. Perrichon, V., Pijolat, M., and Primet, M., *J. Mol. Catal.* **25,** 207 (1984).
28. Dwyer, D. J., and Somorjai, G. A., *J. Catal.* **52,** 291 (1978).
29. Reymond, J. P., Meriaudeau, P., and Teichner, S. J., *J. Catal.* **75,** 39 (1982).
30. Kuivila, C. S., Stair, P. C., and Butt, J. B., *J. Catal.* **118,** 299 (1989).
31. Dictor, R. A., and Bell, A. T., *J. Catal.* **97,** 121 (1986).